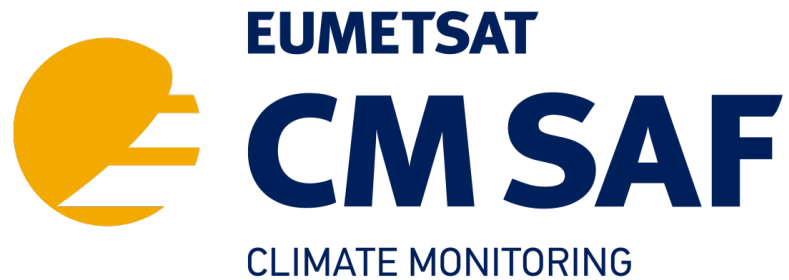


**EUMETSAT Satellite Application Facility on Climate Monitoring**



**Algorithm Theoretical Basis Document  
Meteosat latent and sensible heat fluxes**

Doi:

CM-23811

Reference Number:


SAF/CM/RMI/ATBD/MET/LEH/1.2

Issue/Revision Index:


1.2

Date:

30.05.2023

	<b>Algorithm Theoretical Basis Document.</b>	Doc.No: SAF/CM/RMIB/ATBD/MET/LEH/1.2
	<b>Meteosat Latent and Sensible heat fluxes - Edition 1</b>	Issue: 1.2
		Date: 30.05.2023

### Document Signature Table

	Name	Function	Signature	Date
<b>Author</b>	William Moutier	CM SAF Scientist		
	Françoise Gellens-Meulenberghs	CM/LSA SAF Scientist		
	Alirio Arboleda	CM/LSA SAF Scientist		
	Miguel Barrios	CM/LSA SAF Scientist		
	Nicolas Ghilain	CM SAF Scientist		
	Nicolas Clerboux	CM SAF Scientist		
<b>Editor</b>				
<b>Approval</b>				
<b>Release</b>				


### Distribution List

Internal Distribution	
Name	No. Copies
DWD / Archive	

External Distribution		
Company	Name	No. Copies
Public		

### Document Change Record

Issue/Revision	Date	DCN No.	Changed Pages/Paragraphs
1.0	30/05/20	SAF/CM/RMIB/ATBD/MET/LEH/1	First official version.

	<b>Algorithm Theoretical Basis Document.</b> <b>Meteosat Latent and Sensible heat fluxes - Edition 1</b>	Doc.No: SAF/CM/RMIB/ATBD/MET/LEH/1.2
		Issue: 1.2
		Date: 30.05.2023

1.1	15/08/20	SAF/CM/RMIB/ATBD/MET/LEH/1.1	Included suggestions from reviewers during PCR 3.9.
1.2	05/30/2023	SAF/CM/RMIB/ATBD/MET/LEH/1.2	Included suggestions from reviewers during DRR 3.9.

### Applicable Documents


Reference	Title	Code
AD 1	CM SAF Product Requirements Document	SAF/CM/DWD/PRD/3.9

### Reference Documents

Reference	Title	Code
RD 1	LSA SAF Algorithm Theoretical Basis Document, For Evapotranspiration and Surface Fluxes version 1.1	SAF/LAND/IM/ATBD_ETv2HLE/1.1
RD 2	LSA SAF Validation Report. For Evapotranspiration & Surface Fluxes , version 1.1	SAF/LAND/RMI/VR/1.1
RD 3	LSA SAF Product User Manual. For Evapotranspiration and Surface Fluxes version 1.1	SAF/LAND/RMI/PUM/ET&SF/1.1
RD 4	Algorithm Theoretical Basis Document. Meteosat Surface Radiative Balance Edition 1	SAF/CM/MeteoSwiss/ATBD/MET/SR B/1

## Table of Contents

<b>1. THE EUMETSAT SAF ON CLIMATE MONITORING (CM SAF)</b> .....	<b>7</b>
<b>2. INTRODUCTION</b> .....	<b>8</b>
2.1 Features of the CDR .....	8
2.2 Algorithm overview.....	9
<b>3 DATA</b> .....	<b>13</b>
3.1 MeteoSat data.....	13
3.2 ESA CCI Land Cover dataset .....	13
3.3 Tree height.....	15
3.4 ERA5 dataset.....	15
3.5 LAI GLOMAP dataset .....	19
<b>4 ALGORITHM</b> .....	<b>19</b>
4.1 LAI daily estimation and processing .....	19
4.2 Model description at the tile level .....	20
4.2.1 The surface energy balance .....	20
4.2.2 The Heat flux conduction into the ground .....	21
4.2.3 Latent and Sensible heat flux.....	21
4.3 Calculation at the pixel level.....	26
4.3.1 Instantaneous products.....	26
4.3.2 Iterative solver.....	27
<b>5 SPATIO-TEMPORAL AVERAGING</b> .....	<b>28</b>
5.1 Purpose of the daily and monthly averaging .....	28
5.2 Algorithm overview.....	29
5.3 Algorithm description.....	30
5.3.1 Hourly integration.....	30
5.3.2 Daily mean .....	30
5.3.3 Monthly mean diurnal cycle .....	31
5.3.4 Monthly mean .....	31
5.3.5 Spatial re-gridding.....	31
<b>6 ASSUMPTIONS AND LIMITATIONS</b> .....	<b>32</b>

	<p align="center"><b>Algorithm Theoretical Basis Document.</b>  <b>Meteosat Latent and Sensible heat fluxes - Edition 1</b></p>	<p>Doc.No: SAF/CM/RMIB/ATBD/MET/LEH/1.2  Issue: 1.2  Date: 30.05.2023</p>
---	---	---

**7 REFERENCES..... 32**

**8 GLOSSARY..... 37**

**9 ANNEX..... 41**

**9.1 Difference between LSA SAF and current approach..... 41**

**List of Tables**

Table 2-1: Main features of the CM-23811 data records. .... 8

Table 2-2: Main characteristic of variables used as inputs in the LSA SAF algorithm. .... 9

Table 2-3: Surface types considered by the algorithm and their associated number. .... 12


Table 3-1: Surface types and associated vegetation coverage ( $C_{veg}$  ; %). .... 13

Table 3-2: Minimum stomatal resistance ( $r_{s_{min}}$ ,  $s\ m^{-1}$ ) and, root density distribution ( $R_k$ ) per vegetation type (in %) over the four layers. .... 17

Table 3-3: Values for the volumetric soil moisture in Van Genuchten (1980) and Clapp-Hornberger (1978), field capacity,  $\theta_{fc}$  and permanent wilting point,  $\theta_{pwp}$  ( $m^3\ m^{-3}$ ) that are used in ERA5 (table extracted from ECMWF 2017). .... 19

Table 4-1:  $a_1$  coefficient values used in the equation 17 to calculate  $\beta_i$  for various surface types. .... **Error! Bookmark not defined.**

Table 9-1: Input sources used in the LSA SAF and the CM SAF approach. .... 41

	<p align="center"><b>Algorithm Theoretical Basis Document.</b>  <b>Meteosat Latent and Sensible heat fluxes - Edition 1</b></p>	<p>Doc.No: SAF/CM/RMIB/ATBD/MET/LEH/1.2  Issue: 1.2  Date: 30.05.2023</p>
---	---	---

## List of Figures

Figure 2-1 Description of the three successive modules, tasks and inputs to produce instantaneous surface heat fluxes, evapotranspiration and averaged values. .... 11

**Figure 2-2** Example of a pixel unit composed of 4 tiles: forest, grass, crops and bare soil. .... 12

Figure 3-1: ESA-CCI Land Cover dataset pre-processing flowchart. Processing performed with the ESA-CCI toolbox is highlighted in blue and in green when an external program has been used. .... 15

Figure 2: Variation of the fraction of unfrozen soil water ( $f_{liq}$ ) according to the soil temperature ( $slt$ )..... 17

Figure 3-3: Flowchart describing ERA5 data process. .... 18


Figure 5: The Jarvis function  $f_1$  as a function of the Surface Incoming Shortwave radiation ( $SIS; W m^{-2}$ ) ..... 25

Figure 4-6: Flowchart illustration of the iterative solving process. The central blocks correspond to the 4 dominant tiles per pixel. The iteration is done until convergence of the pixel averaged values of H, LE and  $T_{sk}$ ..... 28

Figure 5-1: Overview flowchart for the averaging. The 'daily flag' indicates if the criterion on the maximum number of successive missing repeat cycles is met or not. .... 29

Figure 5-2: Graphical representation of hourly integration using linear interpolation between measurements..... 30

Figure 5-3 : Averaging strategy: from the hourly integrated data to the daily mean, to the monthly mean diurnal cycle and to the monthly mean product..... 31

	<p align="center"><b>Algorithm Theoretical Basis Document.</b></p> <p align="center"><b>Meteosat Latent and Sensible heat fluxes - Edition 1</b></p>	<p>Doc.No: SAF/CM/RMIB/ATBD/MET/LEH/1.2</p> <p>Issue: 1.2</p> <p>Date: 30.05.2023</p>
---	--	---

## 1. The EUMETSAT SAF on Climate Monitoring (CM SAF)


The importance of climate monitoring with satellites was recognized in 2000 by EUMETSAT Member States when they amended the EUMETSAT Convention to affirm that the EUMETSAT mandate is also to “contribute to the operational monitoring of the climate and the detection of global climatic changes”. Following this, EUMETSAT established within its Satellite Application Facility (SAF) network a dedicated centre, the SAF on Climate Monitoring (CM SAF, <http://www.cmsaf.eu>).

The consortium of CM SAF currently comprises the Deutscher Wetterdienst (DWD) as host institute, and the partners from the Royal Meteorological Institute of Belgium (RMIB), the Finnish Meteorological Institute (FMI), the Royal Meteorological Institute of the Netherlands (KNMI), the Swedish Meteorological and Hydrological Institute (SMHI), the Swiss Federal Office of Meteorology and Climatology (MeteoSwiss), and the Meteorological Service of the United Kingdom (UK MetOffice). Since the beginning in 1999, the EUMETSAT Satellite Application Facility on Climate Monitoring (CM SAF) has developed and will continue to develop capabilities for a sustained generation and provision of Climate Data Records (CDR's) derived from operational meteorological satellites.

In particular, the generation of long-term data sets is pursued. The ultimate aim is to make the resulting data sets suitable for the analysis of climate variability and potentially the detection of climate trends. CM SAF works in close collaboration with the EUMETSAT Central Facility and liaises with other satellite operators to advance the availability, quality and usability of Fundamental Climate Data Records (FCDRs) as defined by the Global Climate Observing System (GCOS). As a major task, the CM SAF utilizes FCDRs to produce records of Essential Climate Variables (ECVs) as defined by GCOS. Thematically, the focus of CM SAF is on ECVs associated with the global energy and water cycle.

Another essential task of CM SAF is to produce data sets that can serve applications related to the new Global Framework of Climate Services initiated by the WMO World Climate Conference-3 in 2009. CM SAF is supporting climate services at national meteorological and hydrological services (NMHSs) with long-term data records but also with data sets produced close to real time that can be used to prepare monthly/annual updates of the state of the climate. Both types of products together allow for a consistent description of mean values, anomalies, variability and potential trends for the chosen ECVs. CM SAF ECV data sets also serve the improvement of climate models both at global and regional scale. As an essential partner in the related international frameworks, in particular WMO Sustained COordinated Processing of Environmental satellite data for Climate Monitoring (SCOPE-CM), the CM SAF - together with the EUMETSAT Central Facility, assumes the role as main implementer of EUMETSAT's commitments in support to global climate monitoring. This is achieved through:

- Application of highest standards and guidelines as lined out by GCOS for the satellite data processing,
- Processing of satellite data within a true international collaboration benefiting from developments at international level and pollinating the partnership with own ideas and standards,
- Intensive validation and improvement of the CM SAF climate data records, • Taking a major role in data set assessments performed by research organisations such as WCRP. This role provides the CM SAF with deep contacts to research organizations that form a substantial user group for the CM SAF CDRs,
- Maintaining and providing an operational and sustained infrastructure that can serve the community within the transition of mature CDR products from the research community into operational environments.

	<p align="center"><b>Algorithm Theoretical Basis Document.</b></p> <p align="center"><b>Meteosat Latent and Sensible heat fluxes - Edition 1</b></p>	<p>Doc.No: SAF/CM/RMIB/ATBD/MET/LEH/1.2</p> <p>Issue: 1.2</p> <p>Date: 30.05.2023</p>
---	--	---

A catalogue of all available CM SAF products is accessible via the CM SAF webpage, <http://www.cmsaf.eu>. Here, detailed information about product ordering, add-on tools, sample programs and documentation is provided.

## 2. Introduction

This CM SAF algorithm targets the quantification of the sensible and latent heat fluxes using input data derived from Meteosat First and Second Generation (MFG/MSG) satellites. The sensible heat flux represents the amount of energy transferred by convection and/or conduction from the surface to the atmosphere (Mito et al., 2012; Pipunic et al., 2008). The amount of energy and water consumed by evaporation and transpiration corresponds to the latent heat flux and the evapotranspiration process (Pipunic et al., 2008; Katul et al., 2012). By materializing the exchange of water and energy from the earth surface to the atmosphere, the latent and sensible heat fluxes control the development of the planetary boundary layer and govern land-atmosphere interaction (Michel et al., 2016; Behrendt et al., 2019). They play a major role in the hydrological cycle (Oki et al., 2006), carbon cycle (Sellers et al., 1997) and surface energy balance (Trenberth et al., 2009). Thus various applications as water resource management, agricultural planning, weather forecasting, drought/flood detection, etc, are possible thanks to their estimations (Fisher, 2017; Liou et al., 2014 and reference there in). For instance, monitoring of H/LE allows the detection of desertification, monsoon circulation and climate change (e.g. Yang et al., 2009; Wang and Li 2011; Shan et al., 2016).

The present document aims at describing the methodology adopted for the CM SAF LE/H algorithm, used for the generation of hourly and daily, monthly and the mean diurnal cycle of sensible heat flux (H) and latent heat flux (Latent Energy, LE). As ancillary products, the evapotranspiration and the skin temperature are also considered.


### 2.1 Features of the CDR

The main features of the CM-23811 data records are summarized in Table 2-1.

**Table 2-1: Main features of the CM-23811 data records.**

<b>Covered period</b>	From 1983 to 2020.
<b>Area Covered</b>	Meteosat Disk (60°N – 60°S; 60°W-60°E)
<b>Temporal characteristics</b>	Fluxes provided as daily mean, monthly mean and monthly mean of the hourly values (diurnal cycle).
<b>Spatial resolution</b>	Regular lat-lon grid with a spatial resolution of (0.05°), i.e., about (5.5 km) <sup>2</sup> at sub-satellite point.
<b>Output quantities</b>	Latent and sensible heat fluxes (W/m <sup>2</sup> ) and evapotranspiration (mm/h)
<b>Validation</b>	Intercomparison with in-situ measurements and other products (e.g. LSA SAF, ERA5, GLDAS)



	<b>Algorithm Theoretical Basis Document.</b>	Doc.No: SAF/CM/RMIB/ATBD/MET/LEH/1.2
	<b>Meteosat Latent and Sensible heat fluxes - Edition 1</b>	Issue: 1.2
		Date: 30.05.2023

**Format**

NetCDF file following the CF convention.

**2.2 Algorithm overview**

The surface latent and sensible heat fluxes, and the evapotranspiration are retrieved by using an adapted version of the methodology developed by the Land Surface Analysis Satellite Application Facility (LSA SAF) v5.0.3 (Ghilain et al., 2011, 2012, 2020; RD 1,2,3). This latter can be described as a Surface Vegetation-Atmosphere Transfer (SVAT) scheme modified to accept input data from external sources (Gellens-Meulenberghs et al., 2006, 2007). The algorithm has been adapted from the Tiled ECMWF (European Centre for Medium-Range Weather Forecasts) Scheme for Surface Exchanges over Land (TESSEL) model (Van den Hurk et al., 2000; Viterbo and Beljaars, 1995) and H-TESEL (Balsamo et al, 2009; Albergel et al, 2012) allowing the use of satellite-based data and numerical weather prediction (NWP) models' outputs (ECMWF reanalysis) as forcing. Observations from the Meteosat Visible and InfraRed Imager (MVISR) and the Spinning Enhanced Visible and InfraRed Imager (SEVIRI), on board of respectively Meteosat First and Second Generation (MFG and MSG), are used as inputs for all radiation components - including the Surface Incoming Solar radiation (SIS), the Surface Albedo (SAL) and the Surface Downward Longwave radiation (SDL) - are jointly retrieved using the CM SAF software "GeoSatClim" (RD 4). All inputs used in the algorithm are listed in the Table 2-2.

The algorithm is composed of three major units (green box in Figure 2-1): 1) pre-processing of the inputs data, in which simple reading, re-projection to the MSG/MFG grid and/or transformation to physical variables directly useable by the model unit are performed; 2) the physical model unit, which derives the instantaneous physical variables related to evapotranspiration and surface heat fluxes from the given inputs and 3) a post-processing module, in which re-gridding to the MSG grid, hourly/monthly/yearly mean/accumulation and monthly mean diurnal cycle are calculated.

**Table 2-2: Main characteristic of variables used as inputs in the LSA SAF algorithm.**

<b>Variable name (shortname; unit)</b>	<b>Source</b>	<b>Spatial resolution</b>	<b>Temporal resolution</b>	<b>Period / Area covered</b>	<b>Reference</b>
Surface Incoming Shortwave radiation (SIS; W m <sup>-2</sup> )	CM-23271	0.05°	15 (MSG)- 30min (MFG)	1983- 2020 / Meteosat disk	RD 4
Surface Downward Longwave radiation (SDL; W m <sup>-2</sup> )					
Surface Albedo (SAL)					
Leaf Area Index (LAI; m <sup>2</sup> m <sup>-2</sup> )	GLOBMAP	0.08°	8 – 16 days	1981-2019 / Global	Lui et al., 2012, 2017
Land Cover (LC)	ESA-CCI	300m	Yearly	1992-2019	ESA 2017; Bontemps et

				/ Global	<i>al., 2012</i>
Tree height ( $h_{tree}$ , m)	NASA/JPL	1 km	Static	Static / Global	<i>Simard et al., 2011</i>
2 metre air temperature ( $T_a$ ; K)					
2 metre dew-point temperature ( $T_d$ ; K)					
10 metre wind ( $U$ & $V$ ; $m\ s^{-1}$ )					
Mean sea level pressure ( $MSL$ , Pa)	ERA-5	0.25°	Hourly	1979-2019 / Global	<i>Hersbach &amp; Dee 2016</i>
Soil type ( $SLT$ )					
Soil temperature level 1->4* ( $stl_i$ ; K)					
Volumetric soil water content layer 1->4* ( $swvl_i$ ; $m^3\ m^{-3}$ )					
Geopotential ( $z$ ; $m^2\ s^{-2}$ )					

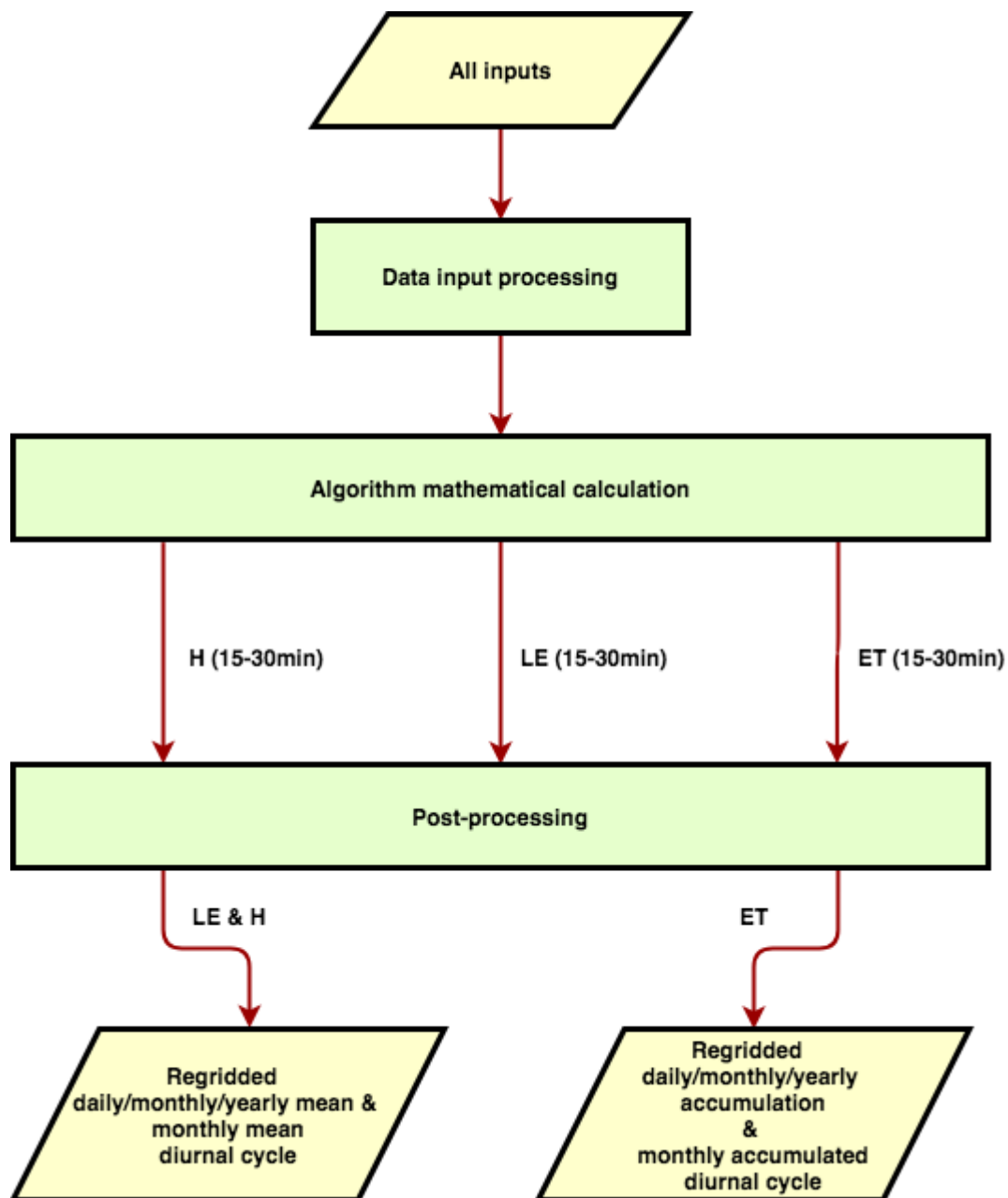


**Figure 2-1** Description of the three successive modules, tasks and inputs to produce instantaneous surface heat fluxes, evapotranspiration and averaged values.

In order to minimise the calculation time, we maximized the upstream pre-processing of the inputs when it is possible. Therefore, upstream pre-processing is performed for ESA-CCI Land Cover and LAI GLOBMAP datasets (see section 3). Concerning the physical model approach, each elementary spatial unit of the algorithm is called *pixel* in reference to the basic unit of the MVIRI/SEVIRI instruments on board of MFG/MSG satellites. Considering the fact that evapotranspiration process and heat exchanges depend on the land cover (surface type), each pixel is split up into a maximum of 4 tiles (**Figure 2-2**). The fraction of each tile being calculated from the LC map. Twelve different land cover types are considered in the algorithm (listed in the Table 2-3). The fluxes are calculated separately for each tile and the final pixel value is obtained by a weighted contribution of all tiles composing it.

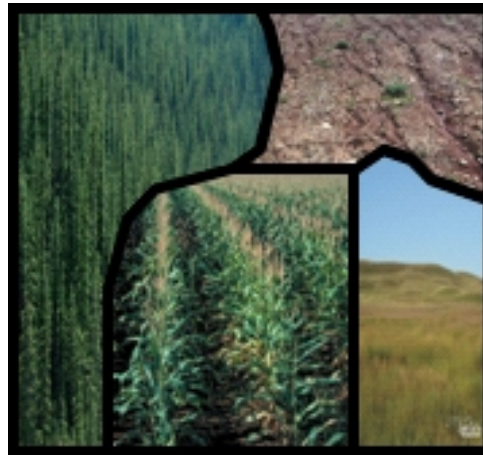


**Figure 2-2** Example of a pixel unit composed of 4 tiles: forest, grass, crops and bare soil.

Finally, the post processing part includes the re-gridding of the outputs to the final grid and the calculation of averaged values for different time ranges. The averaging and re-gridding algorithms used for this last part are described in section 5. Please note that the heat conduction flux into the ground ( $G$ ) will be considered as ancillary dataset as well.

**Table 2-3: Surface types considered by the algorithm and their associated number.**

Surface type number	Surface type
1	Bare soil
2	Snow
3	Deciduous Broadleaved trees
4	Evergreen Needleleaved trees
5	Evergreen Broadleaved trees
6	Crops
7	Irrigated crops
8	Grass
9	Bogs and Marshes
10	Rocks
11	Inland water
12	City

### 3 Data

#### 3.1 MeteoSat data

Calculation of the Surface Incoming Shortwave radiation (SIS), the Surface Downward Longwave radiation (SDL), the emissivity ( $\epsilon$ ) and the Surface Albedo (SAL) are presented in RD4. Please note that the albedo is set to 0.1 for inland water and limited to 0.5 for snow (in case of higher albedo value).

#### 3.2 ESA CCI Land Cover dataset

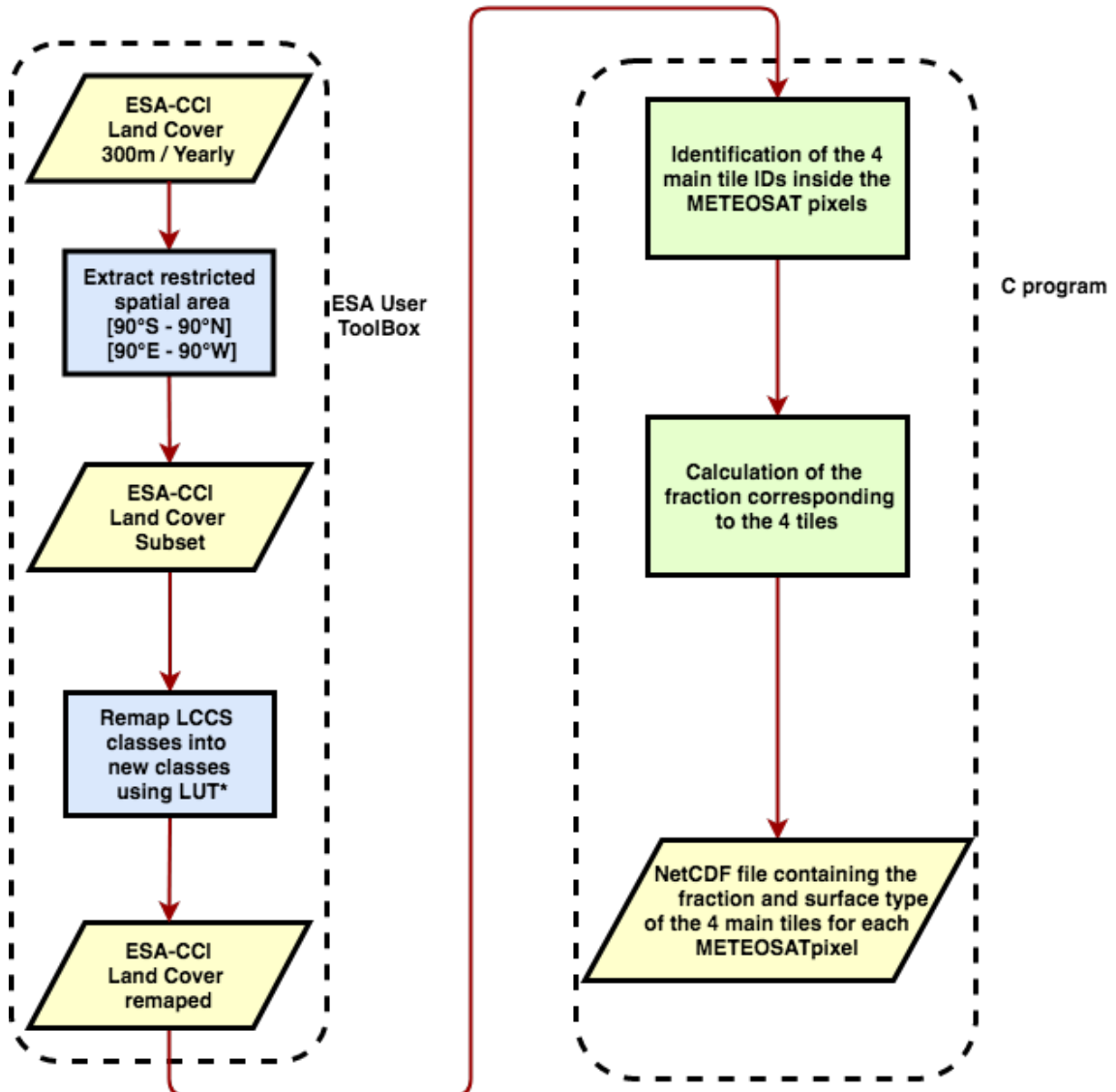
An up-stream pre-processing has been performed to determine the 4 main tiles and to calculate the land cover fraction of each one composing the MFG/MSG pixels. For this purpose, we used the European Spatial Agency (ESA) Climate Change Initiative Land Cover (CCI-LC) climate data record (ESA 2017, Bontemps et al., 2012). The land cover map product is provided globally from 1992 to 2020 at 300m/yearly spatial-temporal resolutions in a Plate Carrée projection. The original dataset is composed of 36 classes allowing a discrimination of the land cover at regional scale. Figure 3-1 presents the steps to perform the pre-processing. The CCI-LC project developed a user toolbox allowing adjustment in the product. With this toolbox (v3.14), area of interest is extracted (latitude: [-90°, 90°]; longitude: [-90°, 90]) and a reclassification from the Land Cover Classification System (LCCS) classes to surface type considered in the algorithm (Table 2-3), based on a Look-Up-Table (adapted from Table 7.2 in ESA 2017), have been performed. Second, the surface type of the 4 main tiles of each MFG/MSG pixel are determined as well as their fraction area ( $\zeta_i$ ).


Note that vegetation types are not 100% covered by vegetation as bare soil contributes to each of them (Table 3-1; based on van den Hurk, et al., 2000). Thus, fraction areas are recalculated by considering the bare soil contribution then, the four main tiles are reordered if needed.

**Table 3-1:** Surface types and associated vegetation coverage ( $c_{veg}$  ; %).

Surface type	$c_{veg}$
<i>Bare soil</i>	0
<i>Snow</i>	0
<i>Deciduous Broadleaved trees</i>	0.9
<i>Evergreen Needleleaved trees</i>	0.9
<i>Evergreen Broadleaved trees</i>	0.99
<i>Crops</i>	0.9

<i>Irrigated crops</i>	0.9
<i>Grass</i>	0.85
<i>Bogs and Marshes</i>	0.6
<i>Rocks</i>	0
<i>Inland water</i>	0
<i>City</i>	0



	<p align="center"><b>Algorithm Theoretical Basis Document.</b> <b>Meteosat Latent and Sensible heat fluxes - Edition 1</b></p>	<p>Doc.No: SAF/CM/RMIB/ATBD/MET/LEH/1.2 Issue: 1.2 Date: 30.05.2023</p>
---	--	---

**Figure 3-1:** ESA-CCI Land Cover dataset pre-processing flowchart. Processing performed with the ESA-CCI toolbox is highlighted in blue and in green when an external program has been used.

### 3.3 Tree height

Tree height ( $h_{tree}$ , m) is a static map over the MFG and MSG period, derived from the global 1km forest canopy height developed at NASA/JPL. This global canopy height map was created using 2005 data from the Geoscience Laser Altimeter System (GLAS) aboard ICESat (Ice, Cloud, and land Elevation Satellite) (Simard et al. 2011). Basically, based on 1 km data, average canopy height has been calculated for each MFG/MSG pixel.

### 3.4 ERA5 dataset

ERA5 variables and respective temporal and spatial resolution to be used have been described previously. The aim of this section is to present various processing steps that are made for each ERA5 variable used in the algorithm. Figure 3-3 presents the followed steps in the processing. Firstly, a bilinear reprojection from native grid to the MFG/MSG grid and a linear interpolation every 15 min is performed. Then, specific calculations are made to get: the total wind speed, the topographic correction for temperature, the relative humidity and the soil moisture.

#### Total wind speed

The vector average wind speed at 10 metres is calculated as:

$$U_a = \sqrt{U^2 + V^2} \quad (1)$$

with,  $U$  and  $V$ , the component vector winds at 10 metres.

#### Topographic correction for temperatures


The general equation to apply topographic correction for 2 metres air temperature ( $T_a$ ) and 2 metres dew point temperature ( $T_{2d}$ ) is defined as following:

$$T_{cor} = T_{uncor} + (\gamma \times (DEM - \frac{z}{g})) \quad (2)$$

where,  $\gamma$  is the reference lapse rate ( $-0.0067 \text{ K m}^{-1}$ ),  $g$  is the gravitational acceleration ( $9.8 \text{ m s}^{-2}$ ),  $z$  the geopotential and DEM the altitude from the digital elevation model (RD 4). In the following,  $T_a$  and  $T_{2d}$  would refer to the corrected values.

#### Relative humidity

The Relative humidity (Rh, unitless) is the ratio between the saturation vapour pressure of  $T_{2d}$  and  $T_a$ :

	<b>Algorithm Theoretical Basis Document.</b> <b>Meteosat Latent and Sensible heat fluxes - Edition 1</b>	Doc.No: SAF/CM/RMIB/ATBD/MET/LEH/1.2 Issue: 1.2 Date: 30.05.2023
---	---	--

$$Rh = \frac{e_w(T_{2d})}{e_w(T_a)} \quad (3)$$

with,

$$e_w(T) = 100 \times 6.112 \times \exp\left(\frac{17.62 \times T}{243.12 + T}\right) \quad (4)$$

where T is the temperature ( $T_{2d}$  or  $T_a$ ) in degree Celsius and  $e_w$  is the vapour pressure at saturation in Pa (Guide To Meteorological Instruments And Methods Of Observation, 2018).

### Soil moisture

For each tile composing the pixel, the soil moisture is obtained by averaging the volumetric soil content at four soil layers weighted by the root density per layer, as indicated in Equation 5.5:

$$\bar{\theta} = \sum_{k=1}^4 R_k \times \max(f_{liq,k} \times swvl_k, \theta_{pwp}) \quad (5)$$

$R_k$  is root density (Table 3-2),  $\theta_{pwp}$  the permanent wilting point (see Table 3-3),  $swvl$  the volumetric soil water of the  $k^{th}$  layer and  $f_{liq,k}$  (Figure 2) the fraction of unfrozen soil water (Viterbo et al., 1999; ECMWF 2017) where the formulation depends on the soil temperature of the  $k^{th}$  layer ( $slt_k$ ).

$$\text{if } slt_k > T_{f1} (= 274.15 \text{ K}): \quad f_{liq,k} = 1 \quad (6)$$

$$\text{if } slt_k < T_{f2} (= 270.15 \text{ K}): \quad f_{liq,k} = 0 \quad (7)$$

$$\text{if } T_{f2} \leq slt_k \leq T_{f1}: \quad f_{liq,k} = 1 - 0.5 \times \left\{ 1 - \sin \left[ \frac{\pi \times (slt_k - 0.5 \times T_{f1} - 0.5 \times T_{f2})}{T_{f1} - T_{f2}} \right] \right\} \quad (8)$$

While  $\bar{\theta}$  could be calculated hourly, the daily mean will be used to be consistent with the (daily) soil moisture retrieved by satellite (see below and section 4). Thus, the inputs in the equations 5 and 8 are daily averaged values.



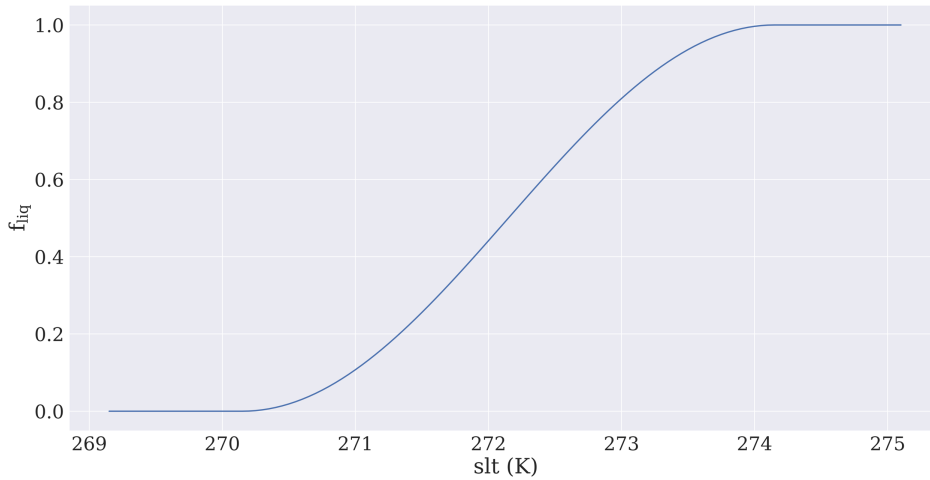


**Figure 2:** Variation of the fraction of unfrozen soil water ( $f_{liq}$ ) according to the soil temperature ( $slt$ ).

**Table 3-2:** Minimum stomatal resistance ( $r_{smin}$ ,  $s\ m^{-1}$ ) and, root density distribution ( $R_k$ ) per vegetation type (in %) over the four layers.

<b>Surface type (number)</b>	<b><math>r_{smin}</math></b>	<b><math>R_1</math></b>	<b><math>R_2</math></b>	<b><math>R_3</math></b>	<b><math>R_4</math></b>
<i>Bare soil (1)</i>	250	100	0	0	0
<i>Snow (2)</i>	-	-	-	-	-
<i>Deciduous Broadleaved trees (3)</i>	350	24	38	31	7
<i>Evergreen Needleleaved trees (4)</i>	180	26	39	29	6
<i>Evergreen Broadleaved trees (5)</i>	200	25	34	27	14
<i>Crops (6)</i>	180	24	41	31	4
<i>Irrigated crops (7)</i>	180	24	41	31	4
<i>Grass (8)</i>	110	35	38	23	4
<i>Bogs and Marshes (9)</i>	250	25	34	27	11
<i>Rocks (10)</i>	1000	-	-	-	-
<i>Inland water (11)</i>	0	-	-	-	-
<i>City (12)</i>	1000	-	-	-	-

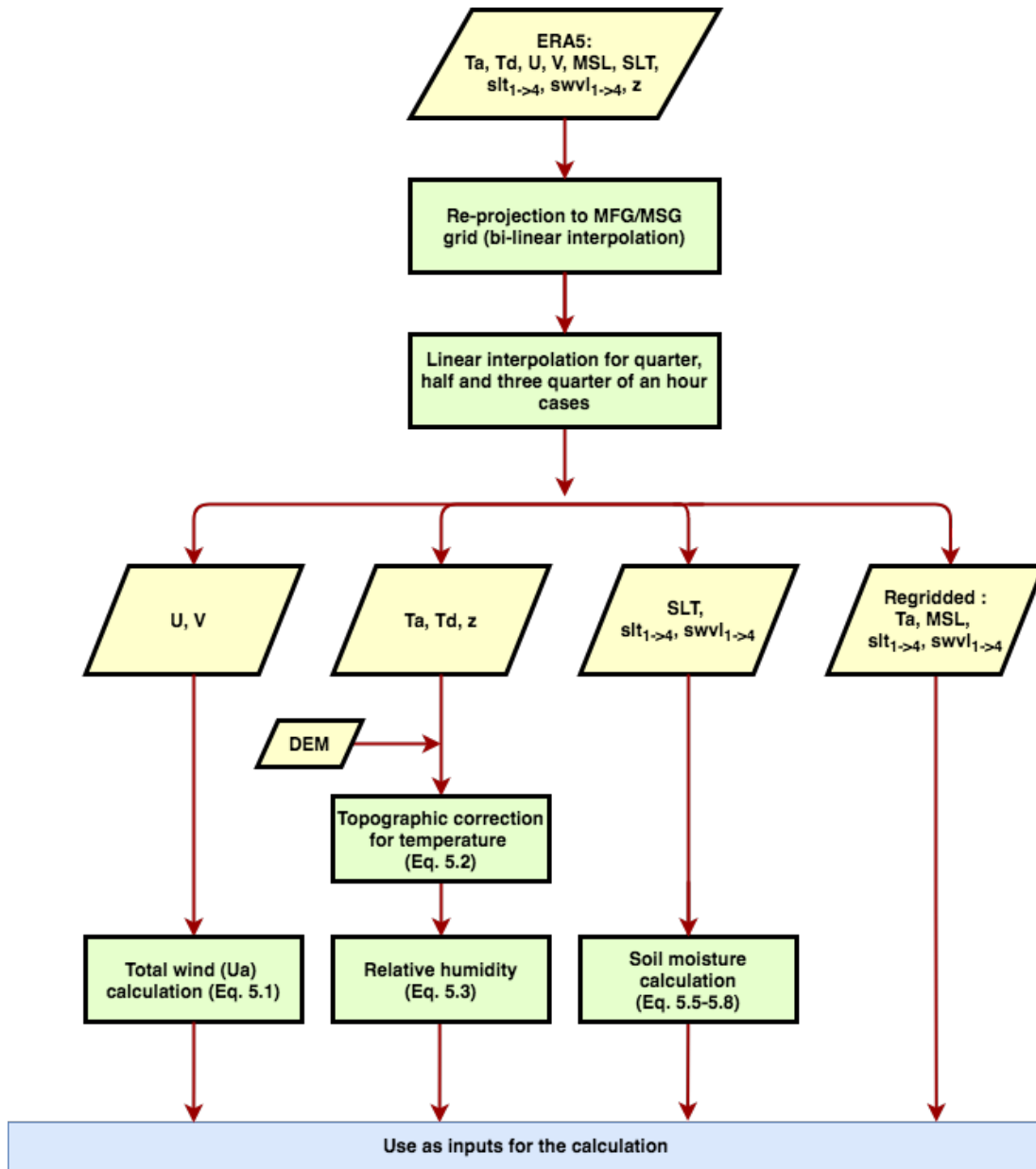


**Figure 3-3:** Flowchart describing ERA5 data process.

**Table 3-3:** Values for the volumetric soil moisture in Van Genuchten (1980) and Clapp-Hornberger (1978), field capacity,  $\theta_{fc}$  and permanent wilting point,  $\theta_{pwp}$  ( $m^3 m^{-3}$ ) that are used in ERA5 (table extracted from ECMWF 2017).

Soil type (texture)	$\theta_{pwp}$	$\theta_{fc}$
Coarse	0.059	0.244
Medium	0.151	0.347
Medium-Fine	0.133	0.383
Fine	0.279	0.448
Very Fine	0.335	0.541
Organic	0.267	0.663
Loamy (CH)	0.171	0.323

### 3.5 LAI GLOBMAP dataset

To get the Leaf Area Index (LAI) value of each MFG/MSG pixel, the long term Global Mapping (GLOBMAP) LAI Version 3 dataset has been chosen. This latter, generated by the Chinese Academy of Sciences, provides half-month (during 1981-2000) or 8 days (during 2001-2020) LAI values over a 39 years' period (1981-2020) with a spatial resolution of  $0.08^\circ$  ( $\sim 8km$ ) (Liu et al., 2011, 2012, 2017). A bilinear reprojection is performed to the MFG/MSG pixel.


## 4 Algorithm

### 4.1 LAI daily estimation and processing

From 8-15 days values, a 'weighted mean' daily value is calculated for each pixel by applying a Gaussian filter to remove potential noise. The Gaussian distribution ( $G$ ) in 1-D has the form:

$$G(\Delta t) = \frac{1}{\sigma\sqrt{2\pi}} \exp\left(-\frac{(\Delta t)^2}{2\sigma^2}\right) \quad (9)$$

where,  $\Delta t$  is the time difference in days between the desired date and the day of the LAI values in the dataset at specific time and  $\sigma$  (equal to 5) is the standard deviation of the distribution. Only images of the dataset being in a time windows of  $\pm 30$  days are used to calculate the final "weighted mean". The following equation is used to make the calculation:

	<p align="center"><b>Algorithm Theoretical Basis Document.</b> <b>Meteosat Latent and Sensible heat fluxes - Edition 1</b></p>	<p>Doc.No: SAF/CM/RMIB/ATBD/MET/LEH/1.2 Issue: 1.2 Date: 30.05.2023</p>
---	--	---

$$LAI_{pix} = \frac{\sum_{n=0}^m G(\Delta t_n)}{\sum_{n=0}^m G(\Delta t_n)} \times LAI_n \quad (10)$$

with,  $m$  the number total of images being in the 30 days time window and  $LAI_n$  the corresponding value at specific time.

In addition, to take into account the surface type, a specific processing is performed to calculate the LAI value of each  $i^{th}$  tile ( $LAI_i$ ). Calculation is performed for all vegetation tiles and a value of 0 is adopted for other surface types. The  $LAI_i$  is calculated for each tile composing the pixel by applying this equation:

$$LAI_i = \alpha \times LAI_{LUT,i} \quad (11)$$

with,

$$\alpha = \frac{LAI_{pix}}{\sum \zeta_i \times LAI_{LUTi}} \quad (12)$$


where,  $\zeta_i$ ,  $LAI_i$ ,  $LAI_{pix}$  and  $LAI_{LUTi}$  are respectively the area fraction of the  $i^{th}$  tile, the LAI of the tile, the LAI of the pixel and the LAI of the tile obtained from a predefined LUT which depend on the surface type of the tile. To build this LUT, four steps have been followed:

- Calculate the monthly mean values.
- Extract all pixels, from the LAI GLOBMAP dataset, considered as “homogeneous”, i.e. where the fraction area of the dominant surface type is higher than 60% (it was not possible to raise the limit higher than 60% as we don’t have enough pixel in this case for grassland type).
- Separate all different vegetation surface types.
- For each surface type, calculate the mean values over four specific areas: South Africa (latitude: [-40.48°, 0.2°], longitude: [7.66°, 79.03°]), North Africa (latitude: [0.19°, 39.39°], longitude: [-21.66°, 79.83°]), Europe (latitude: [34.49°, 81.26°], longitude: [-46.05°, 78.33°]) and South America (latitude: [-37.56°, 12.62°], longitude: [-81.2°, -32.82°]). Thus we get monthly  $LAI_{LUTi}$  values representative of each surface type for various regions of the world.

## 4.2 Model description at the tile level

### 4.2.1 The surface energy balance

The algorithm is an energy balance model aiming to partition the available energy between  $LE$ ,  $H$  and heat conduction flux into the ground ( $G$ ). Thus, for each tile, a closure of the surface energy budget is obtained. The surface energy balance is computed by the algorithm at tile level in a conceptual layer, called skin layer. This latter represents the

	<p style="text-align: center;"><b>Algorithm Theoretical Basis Document.</b> <b>Meteosat Latent and Sensible heat fluxes - Edition 1</b></p>	<p>Doc.No: SAF/CM/RMIB/ATBD/MET/LEH/1.2 Issue: 1.2 Date: 30.05.2023</p>
---	---	---

coverage of the land as a flat layer, without description of the 3-D structure of the canopy. At the tile level  $i^{th}$ , the global surface energy balance equation can be written as:

$$R_{Ni} = H_i + LE_i + G_i \quad (13)$$

with,

$$R_{Ni} = (1 - SAL) \times SIS + \varepsilon \times (SDL - \sigma T_{sk,i}^4) \quad (14)$$

where,  $R_{Ni}$ ,  $SIS$ ,  $SDL$ ,  $T_{sk,i}$ ,  $SAL$ ,  $\sigma$  and  $\varepsilon$  stand respectively for the net radiation, the Surface Incoming Shortwave radiation, the Surface Downward Longwave radiation, the skin temperature of the  $i^{th}$  tile, the surface albedo, the Stefan-Boltzmann constant ( $=5.67 \cdot 10^{-8} \text{ W m}^{-2} \text{ K}^{-4}$ ) and the surface emissivity.

To have typically positive fluxes, at least during day time, the following sign conventions are adopted:

- $R_{Ni}$  is the difference between incoming and outgoing radiation at the surface (SW+LW). A positive value means there is a net absorption of radiant energy in the skin layer.
- The heat  $H$ ,  $LE$  and  $G$  are positive when the energy leaves the skin layer toward the atmosphere ( $H$ ,  $LE$ ) or the ground ( $G$ ).
- The  $SIS$  and  $SDL$  radiative fluxes incident at the surface are always positive.

#### 4.2.2 The Heat flux conduction into the ground

A common choice to parameterize the soil heat flux ( $G_i$ ) is to approximate it as a fraction ( $\beta_i$ ) of the net surface radiation ( $R_{Ni}$ ), assuming that it has a diurnal variation in phase with the net radiation. While different variants based on the same assumption exist in the literature (Choudhury et al., 1987; Bastiaanssen, 1995; Norman et al., 1995; Jacobsen and Hansen, 1999; Friedl, 2002; Kustas et al., 1993; Su, 2002; Santanello and Friedl, 2003), we choose the parameterization of Chehbouni et al., (1996) (Eq. 5), and is adapted for specific land types. Thus,  $G_i$  is defined as following:


$$G_i = \beta_i \times R_{Ni} \quad (15)$$

with,  $\beta_i$  equal to 0.4 for city surface type, 0.2 for rock and bare soil tile, 0.05 for snow tile. Concerning other tiles,  $\beta_i$  is equal to 0.1 for  $R_{Ni} > 0$  and 0.4 for  $R_{Ni} \leq 0$  cases.

#### 4.2.3 Latent and Sensible heat flux

The latent and sensible heat fluxes are obtained via a resistance approach, combining a response of the stomata closure by environmental stress (canopy resistance to transpiration) and the aerodynamic resistance:

$$LE_i = \frac{L_v \rho_a}{(r_a + r_c)} [q_{sat}(T_{sk,i}) - q_a(T_a)] \quad (16)$$

	<p align="center"><b>Algorithm Theoretical Basis Document.</b> <b>Meteosat Latent and Sensible heat fluxes - Edition 1</b></p>	<p>Doc.No: SAF/CM/RMIB/ATBD/MET/LEH/1.2 Issue: 1.2 Date: 30.05.2023</p>
---	--	---

and,

$$H_i = \frac{\rho_a}{r_a} \left[ c_p (T_{sk,i} - T_a) - g z_a \right] \quad (17)$$

where:

- $L_v$  is the latent heat of vaporization ( $\text{J kg}^{-1}$ ),
- $\rho_a$  is the air density ( $\text{kg m}^{-3}$ ),
- $q_a$ , is the specific humidity ( $\text{kg kg}^{-1}$ ) at air temperature  $T_a$  (2m above the surface, in K),
- $q_{sat}$ , is the specific humidity at saturation ( $\text{kg kg}^{-1}$ ) at the surface skin temperature  $T_{sk,i}$  (in K),
- $c_p$  is the heat capacity at constant pressure ( $\text{J K}^{-1} \text{kg}^{-1}$ ),
- $g$  is the gravitational acceleration ( $= 9.8 \text{ m s}^{-2}$ ),
- $z_a$  is the air temperature measurement height ( $= 2 \text{ m}$ ),
- $r_{ai}$  the aerodynamic resistance of the  $i^{\text{th}}$  tile ( $\text{s m}^{-1}$ ).
- $r_{ci}$  the canopy resistance of the  $i^{\text{th}}$  tile ( $\text{s m}^{-1}$ ).

#### 4.2.3.1 Aerodynamic resistance

The aerodynamic resistance is directly connected to the stability of the atmosphere (Eq. 18). Therefore, knowledge of the friction velocity ( $u_{*i}$ ;  $\text{m s}^{-1}$ ) and the Obukhov length ( $L_i$ , m) values are needed and expressed in equations 19 and 20 respectively. The inverse of the aerodynamic resistance is defined as following:

$$\frac{1}{r_a} = \frac{k u_{*i}}{\ln\left(\frac{z_a - d}{z_{0hi}}\right) - \Psi_h\left(\frac{z_a - d}{L_i}\right) + \Psi_h\left(\frac{z_{0hi}}{L_i}\right)} \quad (18)$$


with,

$$u_{*i} = \max \left( 0.2, \frac{k U_a}{\ln\left(\frac{z_t - d_i}{z_{0m_i}}\right) - \Psi_m\left(\frac{z_t - d_i}{L_i}\right) + \Psi_m\left(\frac{z_{0m}}{L_i}\right)} \right) \quad (19)$$

and,

$$L_i = \frac{\rho_a u_{*i}^3}{kg \left( \frac{H_i}{c_p T_a} + 0.608 \frac{LE_i}{L_v} \right)} \quad (20)$$

where,  $d$  is the displacement height,  $k$  the von Kármán constant ( $= 0.4$ ),  $U_a$  the wind speed at 10 meter ( $\text{m s}^{-1}$ ).  $\Psi_h$  and  $\Psi_m$  are, respectively, the sensible heat and momentum

	<p align="center"><b>Algorithm Theoretical Basis Document.</b>  <b>Meteosat Latent and Sensible heat fluxes - Edition 1</b></p>	<p>Doc.No: SAF/CM/RMIB/ATBD/MET/LEH/1.2  Issue: 1.2  Date: 30.05.2023</p>
---	---	---

stability functions, as described in Beljaars and Viterbo (1994);  $z_{om}$  and  $z_{oh}$  are respectively the roughness length for momentum (in meter) and the roughness length for heat (in meter). Finally,  $z_t$  is the air temperature measurement height (= 2 m) and  $z_a$  is the the wind speed measurement height (= 10 m). In practice we consider here a flat surface, having the roughness of the different surface types, without further consideration of the displacement height (= 0 m).

Sensible and latent heat fluxes are needed in equation 20 to compute the Obukhov length, thus the complete system of non-linear equations has to be solved iteratively (see section 4.2 for solving procedure).

The roughness length for momentum is calculated as following (Masson et al, 2003):

$$z_{om} = \max(0.01, 0.13 \times HI) \quad (21)$$

with,  $HI$  (unit m) the height would depend on the vegetation type and LAI as follows.

For bare soil, snow, rocks and inland water cases:

$$HI = 0.001 \quad (22)$$

for crop case:

$$HI = \min\left(1.0, \exp\left(\frac{LAI_i - 3.5}{1.3}\right)\right) \quad (23)$$

for irrigated crop case:

$$HI = \min\left(2.5, \exp\left(\frac{LAI_i - 3.5}{1.3}\right)\right) \quad (24)$$

for grass, bogs and marshes cases:

$$HI = \max\left(0.01, \exp\left(\frac{LAI_i}{6}\right)\right) \quad (25)$$


for city case:

$$HI = 1 \quad (26)$$

for deciduous broadleaved trees, evergreen broadleaved trees and evergreen needleleaved trees cases:

$$HI = \max\left(10, \min(h_{tree}, 30)\right) \quad (27)$$

with,  $h_{tree}$  the height in meter of the trees.

	<p align="center"><b>Algorithm Theoretical Basis Document.</b>  <b>Meteosat Latent and Sensible heat fluxes - Edition 1</b></p>	<p>Doc.No: SAF/CM/RMIB/ATBD/MET/LEH/1.2  Issue: 1.2  Date: 30.05.2023</p>
---	---	---

Finally, the roughness length for heat  $z_{oh}$  is obtained by dividing  $z_{om}$  by 100 for bare soil, deciduous broadleaved trees, evergreen needleleaved trees, rocks and city surface types and, by 10 for other ones (Viterbo et al., 1999; Masson et al. 2003).

#### 4.2.3.2 Canopy resistance to transpiration

The formulation of the canopy resistance  $r_c$  ( $s\ m^{-1}$ ) of the vegetation to transpiration is based on van den Hurk et al. (2000). Change has been made in the parametrisation for crops and non-perennial grasslands to introduce more sensitivity of the model for low green biomass conditions. Thus, the canopy resistance formulation will depend on the surface type.

For vegetation tile cases:

$$r_c = \frac{r_{s,min}}{LAI_i} f_1(SIS) f_2(\bar{\theta}) f_3(D_a) \quad (28)$$

for snow and city cases:

$$r_c = 1000 \quad (29)$$

and, for bog/marches and inland water cases:

$$r_c = 0 \quad (30)$$

Specific parametrisation for bare soil and rock cases will be presented below.

In the equations 28, the Jarvis functions,  $f_{1,2,3}$  parameterize the dependency of the transpiration limitation to basic environmental variables. Thus, the minimum stomatal resistance scaled by  $LAI_i$  set the maximum rate of evapotranspiration observed for each vegetation.  $f_1$  (Figure 4) expresses the limitation due to the illumination of the active canopy (Eq. 31),  $f_2$  the limitation caused by a shortage of water in the soils (Eq. 32-34) and  $f_3$  the limitation for trees due to water vapour deficit in the atmosphere (Eq. 35):

$$f_1(SIS)^{-1} = \min\left(1, \frac{b \times SIS + c}{a \times (b \times SIS + 1)}\right) \quad (31)$$

with,  $a = 0.81$ ,  $b = 0.004$  and  $c = 0.05$  (Van den Hurk et al., 2000).



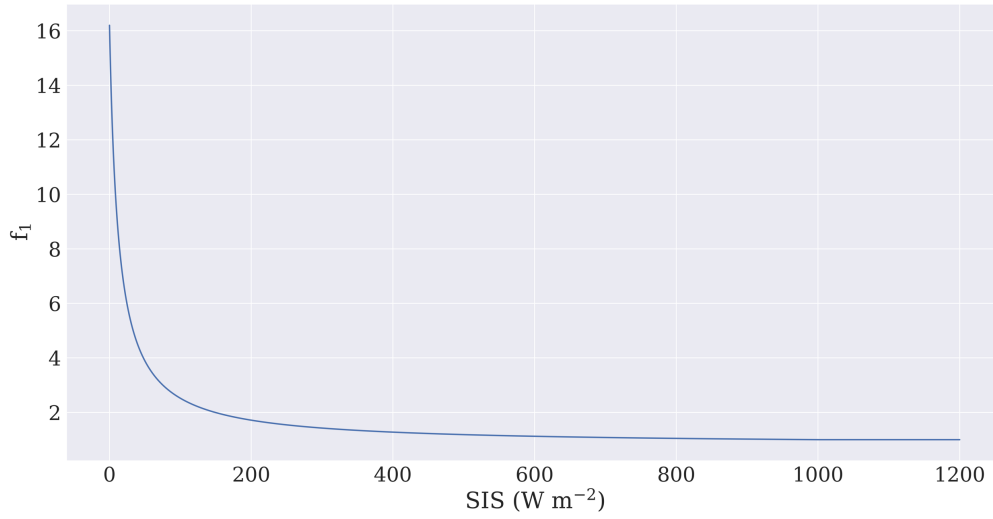


**Figure 4:** The Jarvis function  $f_1$  as a function of the Surface Incoming Shortwave radiation (SIS;  $W m^{-2}$ )

Concerning  $f_2$ ,  $f_3$  and,  $f_4$  :

$$\text{If } \bar{\theta}_i \geq \theta_{fc} \quad f_2(\bar{\theta}_i)^{-1} = 1 \quad (32)$$

$$\text{if } \theta_{pwp} < \bar{\theta}_i < \theta_{fc} \quad f_2(\bar{\theta}_i)^{-1} = \frac{\bar{\theta}_i - \theta_{pwp}}{\theta_{fc} - \theta_{pwp}} \quad (33)$$


$$\text{and, if } \bar{\theta}_i \leq \theta_{pwp} \quad f_2(\bar{\theta}_i)^{-1} = 10^{-10} \quad (34)$$

$$f_3(D_a)^{-1} = \exp(-g_D \times D_a) \quad (35)$$

where,  $g_D$  and  $D_a$  are respectively a sensitivity coefficient for the dependence of the canopy resistance on water vapour pressure deficit (equal to  $3 \cdot 10^{-4} Pa^{-1}$  for Deciduous Broadleaved trees, Evergreen Needleleaved trees and, Evergreen Broadleaved trees cases and 0 for others) and the atmospheric water pressure deficit  $D_a$  which is defined as following:

$$D_a = e_w(T_a) \times (1.0 - Rh) \quad (36)$$

#### 4.2.3.3 Soil surface resistance

	<p align="center"><b>Algorithm Theoretical Basis Document.</b>  <b>Meteosat Latent and Sensible heat fluxes - Edition 1</b></p>	<p>Doc.No: SAF/CM/RMIB/ATBD/MET/LEH/1.2  Issue: 1.2  Date: 30.05.2023</p>
---	---	---

For bare soil and rock tiles, the resistance of the canopy  $r_c$  needed to estimate the latent energy with equation 16 is replaced by  $r_{soil}$  obtained from Eq. 37. A minimum stomatal resistance ( $r_{s,min}$ ; Table 3-2) is associated to bare soil and rock to represent the minimum soil resistance and the only stress for evaporation is due to soil water deficit, via a modified Jarvis function  $f_{2,BS}$  which allows a broader range of soil moisture sensitivity:

$$r_{soil} = r_{s,min} \times f_{2,BS}(f_{liq,1} \times \theta_1) \quad (37)$$

with,

$$f_{2,BS}(f_{liq,1}, \theta_1) = 1 + \left( \frac{1000 \times (\theta_{fc} - \theta_{pwp}) + 1}{\exp(50 \times (f_{liq} \times \theta_1 - \theta_{pwp}))} \right) \quad (38)$$

### 4.3 Calculation at the pixel level

#### 4.3.1 Instantaneous products

Surface heat flux values for the whole pixel are calculated as a weighted contribution of the different tiles:

$$LE = \sum \zeta_i LE_i, \quad (39)$$

$$H = \sum \zeta_i H_i \quad (40)$$

$$T_{sk} = \sum \zeta_i T_{sk,i}$$

and


$$G = \sum \zeta_i G_i \quad (41)$$

with  $\zeta_i$  is the fraction of  $i$  tile in the pixel.  $LE$  and  $H$  are calculated for the whole pixel and are expressed in  $W m^{-2}$ .

From the latent energy, the evapotranspiration ET rate, expressed in  $mm.h^{-1}$ , is given by:

$$ET = \frac{3600 \times LE}{L_v} \quad (42)$$

with  $L_v$  the latent heat of vaporization in  $J Kg^{-1}$  is:

	<p align="center"><b>Algorithm Theoretical Basis Document.</b>  <b>Meteosat Latent and Sensible heat fluxes - Edition 1</b></p>	<p>Doc.No: SAF/CM/RMIB/ATBD/MET/LEH/1.2  Issue: 1.2  Date: 30.05.2023</p>
---	---	---

$$L_v = \left[ 2.501 - 0.00234 \times (T_a - 273.15) \right] \times 10^6 \quad (43)$$

For snow, the latent heat of sublimation is used which includes the additional phase transformation from solid to liquid (fusion):

$$L_s = L_f + L_v \quad (44)$$

where,  $L_f = 0.334 \cdot 10^6 \text{ J kg}^{-1}$ .

### 4.3.2 Iterative solver

For each tile, solving the system of equations (Figure 4-5) requires an iterative method, because of the strong non-linear inter-dependence of the variables  $H$ ,  $LE$ ,  $T_{sk}$  and  $u^*$ . In the implementation, a single point iteration method has been selected for solving the system of equations, assuming neutral stability as a condition. Iterations start with an initialisation of  $H$ ,  $LE$ ,  $T_{sk}$ ,  $u^*$  values and is stopped when the estimates of the three key-variables ( $H$ ,  $LE$ ,  $T_{sk}$ ) are stabilized, using a predefined precision criterion (difference between two successive iterations less than  $0.1 \text{ W m}^{-2}$  for  $H$  and  $LE$  and  $0.01 \text{ K}$  for  $T_{sk}$ ). Initial values are set to  $H = 0 \text{ W m}^{-2}$ ,  $LE = 0 \text{ W m}^{-2}$ ,  $T_{sk} = 273.15 \text{ K}$  and  $u^* = 0.5 \text{ m s}^{-1}$ . Thereafter, the starting point is set from the previous iterated pixel are used. When the number of iterations exceeds 100, the process is stopped and algorithm returns the flag 'not-converged'.

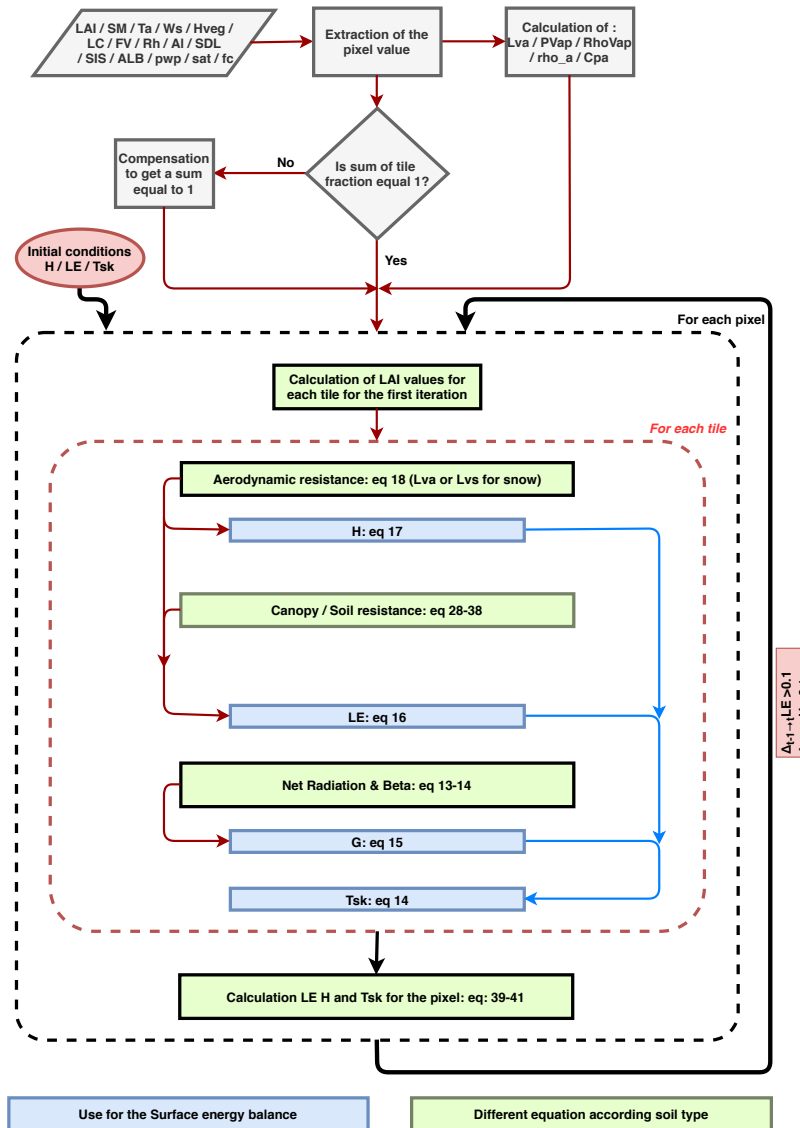


Figure 4-5: Flowchart illustration of the iterative solving process. The central blocks correspond to the 4 dominant tiles per pixel. The iteration is done until convergence of the pixel averaged values of H, LE and  $T_{sk}$ .

## 5 Spatio-temporal averaging

### 5.1 Purpose of the daily and monthly averaging

The purpose of this last part of the processing is to average the output to get the daily mean, monthly mean and monthly mean diurnal cycle of the latent and sensible heat fluxes. Please note that the average procedure is not applied to evapotranspiration as the values are accumulated and not averaged.

First, in the absence of missing data, the averaging algorithm is straightforward: a simple integration would provide the wanted quantities. However, a large number of missing data affects the data record. The daily averaging process accounts for these gaps by interpolating the missing data. However, the interpolation of too many successive missing Meteosat

repeat cycles could bias the daily mean. It is therefore important to estimate the maximum acceptable number of successive missing images which can be interpolated. Second, the outputs are projected on a regular grid at a spatial resolution of 0.05° to maintain consistency with other CM SAF products.

Clearly, a limited amount of successive missing data should be accepted in the averaging algorithm provided that it does not bias the products and improve their RMS difference with the true averaged fluxes. Similarly to the LSA SAF ET-LE/H procedure, missing data are interpolated over a maximum of 3 hours, which correspond to 5 successive missing data for MVIRI and 11 for SEVIRI.

## 5.2 Algorithm overview

The first step of the algorithm performs the sensible and latent heat fluxes averaging in hourly intervals (defined in UTC time). This process is also in charge of the interpolation of the missing data. The daily averaging is then performed from these hourly means (Figure 5-1). A 'daily flag' indicates if the criterion of the 3 maximum successive missing hours is met or not. Then the monthly mean diurnal cycle is computed from the hourly means, excluding days which were flagged as incomplete. A minimum number of 15 days is required to compute the monthly mean for each hourly interval (diurnal cycle). Finally, the monthly mean is evaluated as simple averaging of the diurnal cycle. To avoid introduction of discontinuity in the diurnal cycle, only the days that are not flagged as incomplete are considered.

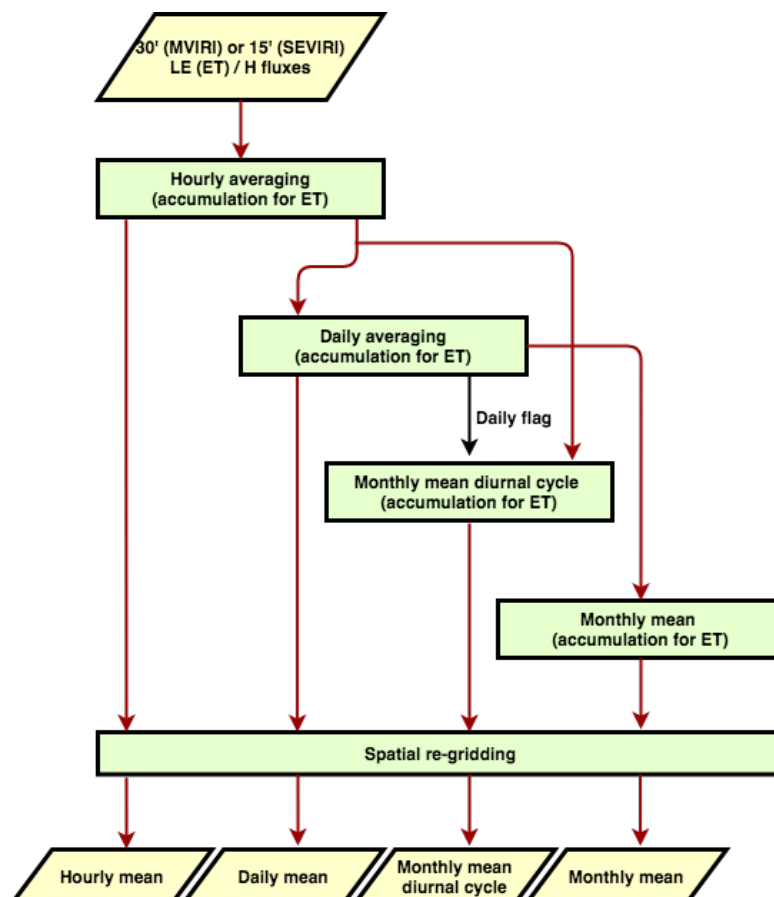


**Figure 5-1:** Overview flowchart for the averaging. The 'daily flag' indicates if the criterion on the maximum number of successive missing repeat cycles is met or not.

## 5.3 Algorithm description

### 5.3.1 Hourly integration

The hourly integration is done with piecewise linear integration between the measurements done during the 1 hour interval, considering also the measurement done just before and just after the interval (Figure 5-2).

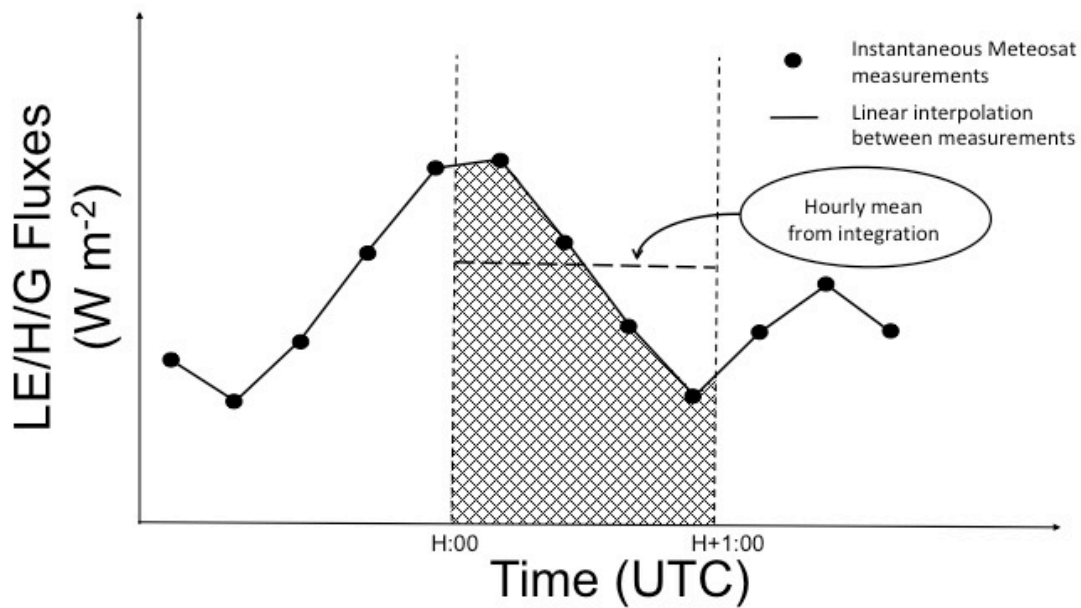


**Figure 5-2:** Graphical representation of hourly integration using linear interpolation between measurements.

As said before, the missing data are temporally interpolated over up to 3-hour.

### 5.3.2 Daily mean

For each pixel, the daily mean is computed from the 24 hourly integrations. In case one or several of these 24 values are missing (it was not possible to fill a gap by interpolation), the daily mean pixel is set to the fill-value. The basic principle of the daily averaging is shown on the Figure 5-3.

If this occurs for all the pixels, the day is flagged as 'incomplete' and no daily mean product will be issued (this flag is also used to discard the day in the monthly averaging, see after).

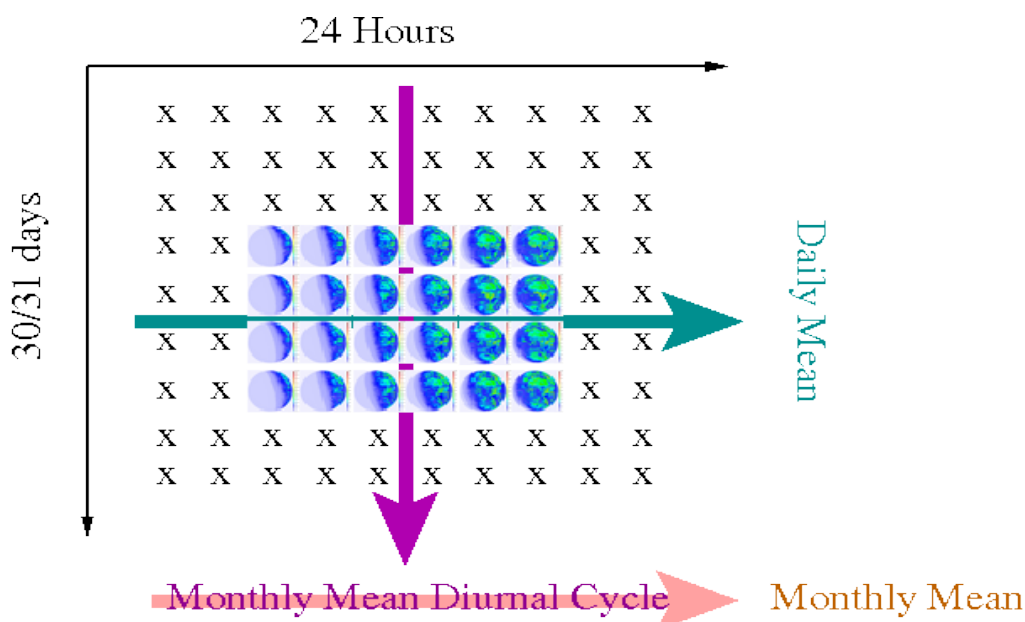


**Figure 5-3 : Averaging strategy: from the hourly integrated data to the daily mean, to the monthly mean diurnal cycle and to the monthly mean product.**

### 5.3.3 Monthly mean diurnal cycle

From the hourly data, the diurnal cycle is computed as the average of the available hourly values for the calendar month. To avoid introduction of discontinuity in the diurnal cycle, only the days which are not flagged as incomplete are considered. A minimum number of 15 days is required to compute each hourly interval of the diurnal cycle (at the pixel level).

If the 15 days criterion of available hourly integrations is not met for all the pixels, the diurnal cycle is flagged as 'incomplete' and no monthly mean will be issued for this hourly interval.


### 5.3.4 Monthly mean

Finally, the monthly mean is evaluated as simple averaging of the diurnal cycle. In case one or several of the 24 monthly 1-hourly means are missing (it was set to incomplete), the monthly mean pixel is set to the fill-value. If this occurs for all the pixels, the month is flagged as 'incomplete' and no monthly mean product is issued.

### 5.3.5 Spatial re-gridding

To ensure consistency with other CM SAF products, ET, LE and H products are re-gridded on a common regular latitude-longitude grid at a spatial resolution of 0.05°. To perform the transformation, a twin target image is built in which each target pixel has a list of the corresponding pixels in the source image and their associated weights. The re-gridding is performed supposing the energy (density of flux) equally distributed in the original pixel. This assumption allows estimating the re-gridded pixel flux using the surface intersection as weighting of the original pixel flux densities.

After re-gridding, the spatial coverage may be limited, e.g. to 60°N - 60°S and 60°W- 60°E. This will be decided in view of the validation results.

	<p align="center"><b>Algorithm Theoretical Basis Document.</b></p> <p align="center"><b>Meteosat Latent and Sensible heat fluxes - Edition 1</b></p>	<p>Doc.No: SAF/CM/RMIB/ATBD/MET/LEH/1.2</p> <p>Issue: 1.2</p> <p>Date: 30.05.2023</p>
---	--	---

## 6 Assumptions and limitations

- In the algorithm, only limited number of plant functional types is considered which is the first assumption made in it.
- The land cover is available yearly and, it does not take into account potential variation of the land cover over the year. In addition, the land cover is considered constant between 1983 and 1992, as the ESA CCI Land Cover dataset do not provide the information over this period.
- The tree height considered is a static file for both periods, which is a limitation as, similarly to the land cover, no potential variation is considered.
- The approach used to calculate the LAI of each tile depends on the fraction of each tile and the use of a LUT. First, the LUT is constant for large Area (Europe, North Africa, South Africa and South America) and may suffer of local variation of the LAI according to the surface type. Second, use the fraction of the tile may induce too low and too high values of LAI if errors are present in the Land cover dataset.
- The validity of the rescaling from the soil moisture index to volumetric unit would depend on the accuracy of ERA5 and the good capture of driest and wettest cases.
- Use daily soil moisture can be an important limitation in hourly outputs when strong precipitation events occurred during the day.
- The algorithm is not entirely based on remote sensing data, and the resulting dataset may be constrained by the Land Surface Model used for the retrieval. This has to be kept in mind when using data, in particular to evaluate models (NWP, climate, land surface, reanalysis, etc.).
- Value obtained from the iteration procedure is potentially a local minimum and not the “truth” value obtained after convergence.


## 7 References

Albergel, C., Balsamo, G., De Rosnay, P., Muñoz-Sabater, J., & Boussetta, S. (2012). A bare ground evaporation revision in the ECMWF land-surface scheme: evaluation of its impact using ground soil moisture and satellite microwave data. *Hydrology and Earth System Sciences*, 16(10), 3607-3620, ISO 690; doi:10.5194/hess-16-3607-2012.

Albergel, C., Rüdiger, C., Pellarin, T., Calvet, J. C., Fritz, N., Froissard, F., Suquia, D., Petitpa, A., Piguet, B., & Martin, E. (2008). From near-surface to root-zone soil moisture using an exponential filter: an assessment of the method based on in-situ observations and model simulations. *Hydrology and Earth System Sciences*, 12, 1323–1337, doi:10.5194/hess-12-1323-2008

Balsamo, G., Beljaars, A., Scipal, K., Viterbo, P., van den Hurk, B., Hirschi, M., & Betts, A. K. (2009). A revised hydrology for the ECMWF model: Verification from field site to terrestrial water storage and impact in the Integrated Forecast System. *Journal of hydrometeorology*, 10(3), 623-643, doi:10.1175/2008JHM1068.1



	<p align="center"><b>Algorithm Theoretical Basis Document.</b>  <b>Meteosat Latent and Sensible heat fluxes - Edition 1</b></p>	<p>Doc.No: SAF/CM/RMIB/ATBD/MET/LEH/1.2  Issue: 1.2  Date: 30.05.2023</p>
---	---	---

Bastiaanssen, W. G. M. (1995). Regionalization of surface flux densities and moisture indicators in composite terrain. A remote sensing approach under clear skies in Mediterranean climates, 271.

Behrendt, A., Wulfmeyer, V., Senff, C., Muppa, S. K., Späth, F., Lange, D., ... & Wieser, A. (2019). Observation of sensible and latent heat flux profiles with lidar. *Atmos. Meas. Tech. Discuss.*

Beljaars, A. C., Viterbo, P. (1994). The sensitivity of winter evaporation to the formulation of aerodynamic resistance in the ECMWF model. *Boundary-Layer Meteorology*, 71(1-2), 135-149. doi:10.1007/BF00709223

Bontemps, S., Herold, M., Kooistra, L., Van Groenestijn, A., Hartley, A., Arino, O., Moreau, I., & Defourny, P. (2012). Revisiting land cover observation to address the needs of the climate modeling community. *Biogeosciences*, 9(6), doi:10.5194/bg-9-2145-2012

Ceballos, A., Scipal, K., Wagner, W., & Martínez-Fernández, J. (2005). Validation of ERS scatterometer-derived soil moisture data in the central part of the Duero Basin, Spain. *Hydrological Processes: An International Journal*, 19(8), 1549-1566.


Chebouni, A., Seen, D. L., Njoku, E. G., & Monteny, B. (1996). A coupled hydrological and ecological modelling approach to examine the relationship between radiative and aerodynamic surface temperature over sparsely vegetated surfaces. *Remote Sens. Environ.*, 58, 177-186.

Choudhury, B. J., Idso, S. B., & Reginato, R. J. (1987). Analysis of an empirical model for soil heat flux under a growing wheat crop for estimating evaporation by an infrared-temperature based energy balance equation. *Agricultural and Forest Meteorology*, 39(4), 283-297, doi:10.1016/0168-1923(87)90021-9

Clapp, R. B., & Hornberger, G. M. (1978). Empirical equations for some soil hydraulic properties. *Water resources research*, 14(4), 601-604, doi:10.1029/WR014i004p00601C

Dorigo, W. A., Gruber, A., De Jeu, R. A. M., Wagner, W., Stacke, T., Loew, A., ... & Kidd, R. (2015). Evaluation of the ESA CCI soil moisture product using ground-based observations. *Remote Sensing of Environment*, 162, 380-395, doi:10.1016/j.rse.2014.07.023

Dorigo, W., Wagner, W., Albergel, C., Albrecht, F., Balsamo, G., Brocca, L., ... & Haas, E. (2017). ESA CCI Soil Moisture for improved Earth system understanding: State-of-the art and future directions. *Remote Sensing of Environment*, 203, 185-215, doi:10.1016/j.rse.2017.07.001

	<p align="center"><b>Algorithm Theoretical Basis Document.</b>  <b>Meteosat Latent and Sensible heat fluxes - Edition 1</b></p>	<p>Doc.No: SAF/CM/RMIB/ATBD/MET/LEH/1.2  Issue: 1.2  Date: 30.05.2023</p>
---	---	---

ECMWF. Part IV: Physical processes. In IFS Documentation CY43R3; Number 4 in IFS Documentation; ECMWF: Reading, UK, 2017.

ESA. Land Cover CCI Product User Guide Version 2. Tech. Rep. (2017). Available at: [maps.elie.ucl.ac.be/CCI/viewer/download/ESACCI-LC-Ph2-PUGv2\\_2.0.pdf](https://maps.elie.ucl.ac.be/CCI/viewer/download/ESACCI-LC-Ph2-PUGv2_2.0.pdf)

Fisher, J. B., Melton, F., Middleton, E., Hain, C., Anderson, M., Allen, R., ... & Kilic, A. (2017). The future of evapotranspiration: Global requirements for ecosystem functioning, carbon and climate feedbacks, agricultural management, and water resources. *Water Resources Research*, 53(4), 2618-2626.

Friedl, M. A. (2002). Forward and inverse modeling of land surface energy balance using surface temperature measurements. *Remote sensing of environment*, 79(2-3), 344-354, doi:10.1016/S0034-4257(01)00284-X

Gellens-Meulenberghs, F., Arboleda, A., & Ghilain, N. (2006, March). Status of development of the LSA-SAF evapotranspiration product. In Proc. 2nd LSA-SAF Training Workshop (pp. 8-10).

Gellens-Meulenberghs, F., Arboleda, A., & Ghilain, N. (2007). Towards a continuous monitoring of evapotranspiration based on MSG data. *IAHS PUBLICATION*, 316, 228.


Ghilain, N., Arboleda, A., & Gellens-Meulenberghs, F. (2011). Evapotranspiration modelling at large scale using near-real time MSG SEVIRI derived data. *Hydrology & Earth System Sciences*, 15(3), doi:10.5194/hess-15-771-2011

Ghilain, N., Arboleda, A., Sepulcre-Canto, G., Batelaan, O., Ardo, J., & Gellens-Meulenberghs, F. (2012). Improving evapotranspiration in a land surface model using biophysical variables derived from MSG/SEVIRI satellite, doi:10.5194/hess-16-2567-2012

Ghilain, N., Arboleda, A., Batelaan, O., Ardö, J., Trigo, I., Barrios, J. M., & Gellens-Meulenberghs, F. (2019). A new retrieval algorithm for soil moisture index from thermal infrared sensor on-board geostationary satellites over Europe and Africa and its validation. *Remote Sensing*, 11(17), 1968, doi: 10.3390/rs11171968

Ghilain, N., Arboleda, A., Barrios, J. M., & Gellens-Meulenberghs, F. (2020). Water interception by canopies for remote sensing based evapotranspiration models. *International Journal of Remote Sensing*, 41(8), 2934-2945, doi:10.1080/01431161.2019.1698072

Guide To Meteorological Instruments And Methods Of Observation (2018). Geneva, Switzerland: World Meteorological Organization, p.188.

	<p align="center"><b>Algorithm Theoretical Basis Document.</b>  <b>Meteosat Latent and Sensible heat fluxes - Edition 1</b></p>	<p>Doc.No: SAF/CM/RMIB/ATBD/MET/LEH/1.2  Issue: 1.2  Date: 30.05.2023</p>
---	---	---

Hersbach, H., & Dee, D. (2016). ERA5 reanalysis is in production, ECMWF Newsletter 147, ECMWF. Reading, UK.

Jacobsen, A. (1999). Estimation of the soil heat flux/net radiation ratio based on spectral vegetation indexes in high-latitude Arctic areas. *International Journal of Remote Sensing*, 20(2), 445-461, doi:10.1080/014311699213532

Katul, G. G., Oren, R., Manzoni, S., Higgins, C., & Parlange, M. B. (2012). Evapotranspiration: a process driving mass transport and energy exchange in the soil-plant-atmosphere-climate system. *Reviews of Geophysics*, 50(3).

Kustas, W. P., Daughtry, C. S., & Van Oevelen, P. J. (1993). Analytical treatment of the relationships between soil heat flux/net radiation ratio and vegetation indices, doi:10.1016/0034-4257(93)90052-Y

Liou, Y. A., & Kar, S. K. (2014). Evapotranspiration estimation with remote sensing and various surface energy balance algorithms—A review. *Energies*, 7(5), 2821-2849.

Liu, Y. Y., Parinussa, R. M., Dorigo, W. A., De Jeu, R. A., Wagner, W., Van Dijk, A., ... & Evans, J. (2011). Developing an improved soil moisture dataset by blending passive and active microwave satellite-based retrievals, doi:10.5194/hess-15-425-2011


Liu, Y., Liu, R., & Chen, J. M. (2012). Retrospective retrieval of long-term consistent global leaf area index (1981–2011) from combined AVHRR and MODIS data. *Journal of Geophysical Research: Biogeosciences*, 117(G4), doi:10.1029/2012JG002084

Liu, Y., Liu, R., Pisek, J., & Chen, J. M. (2017). Separating overstory and understory leaf area indices for global needleleaf and deciduous broadleaf forests by fusion of MODIS and MISR data. *Biogeosciences*, 14(5), 1093, doi:10.5194/bg-14-1093-2017

Martins, J., Trigo, I. F., Ghilain, N., Jimenez, C., Göttsche, F. M., Ermida, S. L., ... & Arboleda, A. (2019). An All-Weather Land Surface Temperature Product Based on MSG/SEVIRI Observations. *Remote Sensing*, 11(24), 3044, doi: 10.3390/rs11243044

Masson, V., Champeaux, J. L., Chauvin, F., Meriguet, C., & Lacaze, R. (2003). A global database of land surface parameters at 1-km resolution in meteorological and climate models. *Journal of climate*, 16(9), 1261-1282.

Michel, D., Jiménez, C., Miralles, D. G., Jung, M., Hirschi, M., Ershadi, A., ... & Seneviratne, S. I. (2016). The WACMOS-ET project—Part 1: Tower-scale evaluation of four remote-sensing-based evapotranspiration algorithms. *Hydrology and Earth System Sciences*, 20(2), 803-822.

	<p align="center"><b>Algorithm Theoretical Basis Document.</b>  <b>Meteosat Latent and Sensible heat fluxes - Edition 1</b></p>	<p>Doc.No: SAF/CM/RMIB/ATBD/MET/LEH/1.2  Issue: 1.2  Date: 30.05.2023</p>
---	---	---

Mito, C. O., Boiyo, R. K., & Laneve, G. (2012). A simple algorithm to estimate sensible heat flux from remotely sensed MODIS data. *International journal of remote sensing*, 33(19), 6109-6121.

Norman, J. M., Kustas, W. P., & Humes, K. S. (1995). Source approach for estimating soil and vegetation energy fluxes in observations of directional radiometric surface temperature. *Agricultural and Forest Meteorology*, 77(3-4), 263-293, doi:10.1016/0168-1923(95)02265-Y

Oki, T., & Kanae, S. (2006). Global hydrological cycles and world water resources. *science*, 313(5790), 1068-1072.

Pipunic, R. C., Walker, J. P., & Western, A. (2008). Assimilation of remotely sensed data for improved latent and sensible heat flux prediction: A comparative synthetic study. *Remote Sensing of Environment*, 112(4), 1295-1305.

Santanello Jr, J. A., & Friedl, M. A. (2003). Diurnal covariation in soil heat flux and net radiation. *Journal of Applied Meteorology*, 42(6), 851-862, doi:10.1175/1520-0450(2003)042<0851:DCISHF>2.0.CO;2

Sellers, P. J., Dickinson, R. E., Randall, D. A., Betts, A. K., Hall, F. G., Berry, J. A., ... & Sato, N. (1997). Modeling the exchanges of energy, water, and carbon between continents and the atmosphere. *Science*, 275(5299), 502-509.


Shan, N., Shi, Z., Yang, X., Zhang, X., Guo, H., Zhang, B., & Zhang, Z. (2016). Trends in potential evapotranspiration from 1960 to 2013 for a desertification-prone region of China. *International Journal of Climatology*, 36(10), 3434-3445.

Simard, M., Pinto, N., Fisher, J. B., & Baccini, A. (2011). Mapping forest canopy height globally with spaceborne lidar. *Journal of Geophysical Research: Biogeosciences*, 116(G4), doi: 10.1029/2011JG001708

Su, Z. (2002). The Surface Energy Balance System (SEBS) for estimation of turbulent heat fluxes. *Hydrology and earth system sciences*, 6(1), 85-99.

Trenberth, K. E., Fasullo, J. T., & Kiehl, J. (2009). Earth's global energy budget. *Bulletin of the American Meteorological Society*, 90(3), 311-324.

Van den Hurk, B. J. J. M., Viterbo, P., Beljaars, A. C. M., & Betts, A. K. (2000). Offline validation of the ERA40 surface scheme, ECMWF TechMemo 295. Reading, UK.

	<p align="center"><b>Algorithm Theoretical Basis Document.</b> <b>Meteosat Latent and Sensible heat fluxes - Edition 1</b></p>	<p>Doc.No: SAF/CM/RMIB/ATBD/MET/LEH/1.2 Issue: 1.2 Date: 30.05.2023</p>
---	--	---

Van Genuchten, M. T. (1980). A closed-form equation for predicting the hydraulic conductivity of unsaturated soils 1. *Soil science society of America journal*, 44(5), 892-898, doi:10.2136/sssaj1980.03615995004400050002x

Verstraeten, W. W., Veroustraete, F., van der Sande, C. J., Grootaers, I., & Feyen, J. (2006). Soil moisture retrieval using thermal inertia, determined with visible and thermal spaceborne data, validated for European forests. *Remote Sensing of Environment*, 101(3), 299-314, doi: 10.1016/j.rse.2005.12.016

Viterbo, P., & Beljaars, A. C. (1995). An improved land surface parameterization scheme in the ECMWF model and its validation. *Journal of climate*, 8(11), 2716-2748, 10.1175/1520-0442(1995)008<2716:AILSPS>2.0.CO;2

Viterbo, P., Beljaars, A., Mahfouf, J. F., & Teixeira, J. (1999). The representation of soil moisture freezing and its impact on the stable boundary layer. *Quarterly Journal of the Royal Meteorological Society*, 125(559), 2401-2426, doi:10.1002/qj.49712555904

Wang, H., & Li, D. (2011). Correlation of surface sensible heat flux in the arid region of northwestern China with the northern boundary of the East Asian summer monsoon and Chinese summer precipitation. *Journal of Geophysical Research: Atmospheres*, 116(D19).


Wagner, W., Lemoine, G., & Rott, H. (1999). A method for estimating soil moisture from ERS scatterometer and soil data. *Remote sensing of environment*, 70(2), 191-207, doi: 10.1016/S0034-4257(99)00036-X

Wagner, W., Dorigo, W., de Jeu, R., Fernandez, D., Benveniste, J., Haas, E., & Ertl, M. (2012). Fusion of active and passive microwave observations to create an essential climate variable data record on soil moisture. *ISPRS Annals of the Photogrammetry, Remote Sensing and Spatial Information Sciences (ISPRS Annals)*, 7, 315-321.

Yang, K., Qin, J., Guo, X., Zhou, D., & Ma, Y. (2009). Method development for estimating sensible heat flux over the Tibetan Plateau from CMA data. *Journal of applied meteorology and climatology*, 48(12), 2474-2486.


## 8 Glossary

ATBD	Algorithm Theoretical Basis Document
CDF	Cumulative Density Function

	<p align="center"><b>Algorithm Theoretical Basis Document.</b>  <b>Meteosat Latent and Sensible heat fluxes - Edition 1</b></p>	<p>Doc.No: SAF/CM/RMIB/ATBD/MET/LEH/1.2  Issue: 1.2  Date: 30.05.2023</p>
---	---	---

CDOP	Continuous Development and Operations
CDR	Climate Data Record
CDS	Climate Data Store
CM SAF	Satellite Application Facility on Climate Monitoring
DEM	Digital Elevation Model
DWD	Deutscher Wetterdienst (German MetService)
ECMWF	European Center for Medium-Range Weather Forecasts
ERA	ECMWF Re-Analysis
ESA-CCI	European Space Agency ( ESA) Climate Change Initiative (CCI)
ET	EvapoTranspiration
EUMETSAT	European Organisation for the Exploitation of Meteorological Satellites
FC	Field Capacity
GLAS	Geoscience Laser Altimeter System
GLDAS	Global Land Data Assimilation System
GLOBMAP	Global Mapping
H	Sensible heat flux
HR	Heating Rates
ICESat	Ice, Cloud, and land Elevation Satellite
JPL	Jet Propulsion Laboratory
LAI	Leaf Area Index
LC	Land Cover

LCCS	Land Cover Classification System
LE	Latent heat flux
LSA SAF	Land Surface Analysis Satellite Application Facility
LST	Land Surface Temperature
LUT	Look-Up-Table
METEOSAT	Meteorological Satellite(s) series operated by EUMETSAT
MFG	METEOSAT First Generation
MSAVI	Modified Soil Adjusted Vegetation Index
MSG	Meteosat Second Generation
MSL	Mean sea level pressure
MVIRI	METEOSAT Visible and Infrared Imager
NASA	National Aeronautics and Space Administration
NWP	Numerical Weather Prediction
NetCDF	Network Common Data Form
PP	Project Plan
PRD	Product Requirement Document
PUM	Product User Manual
PWP	Permanent Wilting Point
RMIB	Royal Meteorological Institute of Belgium
RR	Requirements Review
$r_{s_{min}}$	minimum stomatal resistance
SAL	Surface Albedo

	<p align="center"><b>Algorithm Theoretical Basis Document.</b>  <b>Meteosat Latent and Sensible heat fluxes - Edition 1</b></p>	<p>Doc.No: SAF/CM/RMIB/ATBD/MET/LEH/1.2  Issue: 1.2  Date: 30.05.2023</p>
---	---	---

SCEM-UA	Shuffled Complex Evolution Metropolis algorithm
SDL	Surface Downward Longwave radiation
SEVIRI	Spinning Enhanced Visible and Infrared Imager
SIS	Surface Incoming Solar radiation
SSM	Surface Soil Moisture
SVAT	Surface Vegetation-Atmosphere Transfer
TESSEL	Tiled ECMWF Scheme for Surface Exchanges over Land
UTC	Coordinated Universal Time



## 9 Annex

### 9.1 Difference between LSA SAF and current approach

Basically, the algorithm calculation part (section 4) is similar to the LSA SAF algorithm V5.0.3. Differences are related to input choices and processing of them. The summarize inputs sources used in the LSA SAF code and the current one. For instance, while three sources are used to get the soil moisture in the current code, two are used in the LSA SAF approach. Other difference can be seen is the retrieval of the LAI of the tile. Indeed, an inversion matrix approach is used in the LSA SAF while an LUT approach is adopted here (see details in section 4 and Ghilain et al., 2012). All details about LSA SAF (pre)processing of the data inputs can be seen in the RD 1-3 documents.

**Table 9-1:** Input sources used in the LSA SAF and the CM SAF approach.

Variable name	CM SAF Source	LSA SAF Source
Surface Incoming Shortwave radiation		LSA SAF
Surface Downward Longwave radiation	CM SAF	LSA SAF
Surface Albedo		LSA SAF
Leaf Area Index	GLOBMAP	LSA SAF
Land Cover	ESA-CCI	ECOCLIMAP
Surface Soil Moisture	ERA-5 / ESA-CCI / LST	H SAF/LST (LSA SAF)
Meteorological field	ERA-5	ECMWF IFS predictions



**Algorithm Theoretical Basis Document.**

**Meteosat Latent and Sensible heat  
fluxes - Edition 1**

Doc.No: SAF/CM/RMIB/ATBD/MET/LEH/1.2

Issue: 1.2

Date: 30.05.2023